

Structures, protonation, and electrochemical properties of diiron dithiolate complexes containing pyridyl-phosphine ligands†

Ping Li,^a Mei Wang,^{*a} Lin Chen,^a Jihong Liu,^a Zhenbo Zhao^a and Licheng Sun^{*a,b}

Received 18th August 2008, Accepted 8th December 2008

First published as an Advance Article on the web 28th January 2009

DOI: 10.1039/b814336f

Diiron complexes containing pyridyl-phosphine ligands, that is, $(\mu\text{-pdt})[\text{Fe}_2(\text{CO})_5\text{L}]$ ($\text{pdt} = \text{S}(\text{CH}_2)_3\text{S}$, $\text{L} = \text{Ph}_2\text{PCH}_2\text{Py}$, **3a**; Ph_2PPy , **3b**) and $(\mu\text{-pdt})[\text{Fe}(\text{CO})_2(\text{PMe}_3)][\text{Fe}(\text{CO})_2\text{L}]$ ($\text{L} = \text{Ph}_2\text{PCH}_2\text{Py}$, **4a**; Ph_2PPy , **4b**) were prepared as model complexes of the $[\text{FeFe}]$ -hydrogenase active site. Protonation of **3a** and **3b** by HOTf afforded the pyridyl-nitrogen protonated products $[\mathbf{3aH}_N][\text{OTf}]$ and $[\mathbf{3bH}_N][\text{OTf}]$, respectively. The molecular structures of **3a**, **3b**, **4a**, **4b**, as well as $[\mathbf{3aH}_N][\text{OTf}]$ and $[\mathbf{3bH}_N][\text{OTf}]$ were confirmed by X-ray diffraction studies, which show that the $\text{Ph}_2\text{PCH}_2\text{Py}$ ligand occupies the basal position both in **3a** and its protonated species $[\mathbf{3aH}_N][\text{OTf}]$, while the Ph_2PPy ligand prefers the apical position in **3b** and $[\mathbf{3bH}_N][\text{OTf}]$. The double protonation process of complex **4b** was monitored by *in situ* IR, ^1H and ^{31}P NMR spectroscopy at low temperature. The spectroscopic evidence indicates that the protonation of **4b** occurs first at the Fe–Fe bond and then at the pyridyl-nitrogen atom. Cyclic voltammograms reveal that protonation of **3a** and **3b** results in a considerable decrease in the overpotential for electrocatalytic proton reduction in the presence of HOTf, while the efficiency is not influenced by protonation. The electrocatalytic efficiency of **4a** for proton reduction in the presence of HOAc in $\text{CH}_3\text{CN}-\text{H}_2\text{O}$ (50 : 1, v/v) is 5 times higher than that in pure CH_3CN .

Introduction

The crystallographic and spectroscopic studies of $[\text{FeFe}]$ -hydrogenases ($[\text{FeFe}]$ -Hases) have revealed that the active site of $[\text{FeFe}]$ -Hases has a simple diiron structure, closely resembling the structure of a well-known diiron dithiolate complex $(\mu\text{-pdt})[\text{Fe}_2(\text{CO})_6]$ ($\text{pdt} = \text{S}(\text{CH}_2)_3\text{S}$).^{1,2} This finding has inspired organometallic chemists to devote more attention to the chemistry of diiron dithiolate complexes. Studies on the diiron dithiolate complexes containing a pendant internal base are of interest for better understanding the mechanism of enzymatic proton reduction and dihydrogen oxidation, and for designing efficient iron-based homogeneous catalysts. A pendant internal base or the

bridging S atom may act as a proton relay to form a proton-hydride diiron dithiolate intermediate,^{3–6} which is an inevitable state in the heterolytic H–H forming/breaking processes at the $[\text{FeFe}]$ -Hase active site (H-cluster). There are two possible basic sites in the H-cluster, that is, the nitrogen atoms in the $\text{SCH}_2\text{NHCH}_2\text{S}$ bridge and the CN^- ligand.^{7,8} The potential function of these pendant bases of the H-cluster in the process of enzymatic dihydrogen generation and uptake is still a problematic issue.

Spectroscopic evidence has proved that the protonation of the bridging nitrogen atom of diiron azadithiolate complexes occurred rapidly,^{9,10} and two nitrogen-protonated products were crystallographically characterized.^{11,12} Recently, two examples of the proton-hydride species of diiron azadithiolate complexes have been reported. The one, formed *in situ* by double protonation of $[(\mu\text{-SCH}_2)_2\text{NH}][\text{Fe}(\text{CO})(\text{dppv})]_2$ ($\text{dppv} = \text{cis-1,2-bis(diphenylphosphino)ethene}$) at -78°C , contains a terminal hydride and a bridging-ammonium centre.⁵ The other proton-hydride species, generated *in situ* by double protonation of $[(\mu\text{-SCH}_2)_2\text{NBn}][\text{Fe}(\text{CO})_2(\text{PMe}_3)]_2$ at 25°C , bears a μ -hydride and an ammonium centre.^{3,4} The proton carried by the bridging nitrogen atom is adjacent to the apical terminal hydride in the proposed structure of the former example (Fig. 1(a)), but it

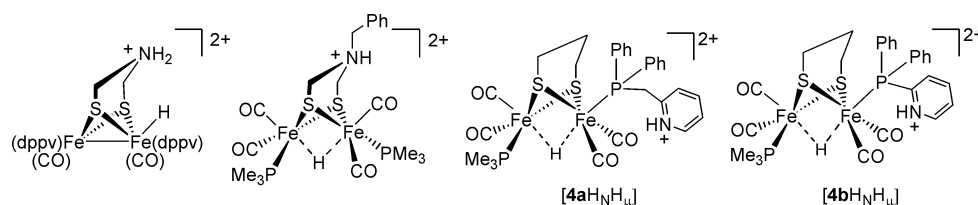


Fig. 1 Possible structures for doubly protonated species of $[(\mu\text{-SCH}_2)_2\text{NH}][\text{Fe}(\text{CO})(\text{dppv})]_2$, $[(\mu\text{-SCH}_2)_2\text{NBn}][\text{Fe}(\text{CO})_2(\text{PMe}_3)]_2$, **4a**, and **4b**.

^aState Key Laboratory of Fine Chemicals, DUT-KTH Joint Education and Research Centre on Molecular Devices, Dalian University of Technology (DUT), Dalian, 116012, China

^bKTH School of Chemical Science and Engineering, Organic Chemistry, 10044, Stockholm, Sweden

† Electronic supplementary information (ESI) available: React-IR spectra for the protonation of **4b** in the presence of HOTf; packing diagrams and geometric parameters of $[\mathbf{3aH}_N][\text{OTf}]$ and $[\mathbf{3bH}_N][\text{OTf}]$; cyclic voltammograms of complex **3b** in the presence of HOAc and HOTf. CCDC reference numbers 643385–643390. For ESI and crystallographic data in CIF or other electronic format see DOI: 10.1039/b814336f

is distant from the μ -hydride in the latter example (Fig. 1(b)). Many experiments have proved that at ambient temperature the protonation of the diiron complexes containing strong electron donating ligands, such as PR_3 ,^{13,14} CN^- ,¹⁵ CNR ,¹⁶ N-heterocyclic carbene (NHC),¹⁷ and 1,10-phenanthroline,¹⁸ generates only the μ -hydride diiron complexes. Although the $[\text{Fe}^{\text{II}}(\mu\text{-H})\text{Fe}^{\text{II}}]$ species exhibit no inherent reactivity toward proton reduction, some of them show H/D exchange activity with D_2 and catalytic activity for H/D scrambling between D_2O and H_2 in the presence of light.¹⁴ The results of density functional studies on heterolytic H–H forming/breaking at the diiron sub-cluster suggest that $[\text{Fe}^{\text{II}}(\mu\text{-H})\text{Fe}^{\text{II}}]$ species may act as an intermediate state in the catalytic cycle of the H-cluster.^{19,20} Supposing that a μ -hydride diiron species is involved in the H–H forming/breaking process, the diiron model with a pendant basic site in a σ -donating ligand might be catalytically preferred over that with a secondary amine in the 2-azapropane-1,3-dithiolato (adt) bridge, considering the distance between the μ -hydride and the proton carried by the pendant base.

The pyridyl group has been introduced to the diiron model complexes, either as part of the chelating ligand or as a pendant arm tethered to the central carbon of the pdt bridge,^{21–24} which gives an example for the protonation competition of the pyridyl group and the Fe–Fe bond. We designed diiron complexes containing pyridyl-phosphine ligands, $\text{Ph}_2\text{PCH}_2\text{Py}$ and Ph_2PPy , in which the pyridyl nitrogen atom may act as a proton relay similar to the bridging nitrogen atom of the adt bridge.^{3–5,9–12} In terms of the turnstile rotation of the ligands and the rotation around the Fe–P and P–C (Py) single bonds, the distance between the pyridyl-nitrogen and the μ -hydride is changeable for the model complexes **4a** and **4b** (Fig. 1). The flexible position of the pendant base towards the μ -hydride of the protonated diiron complex could benefit the intramolecular proton–hydride combination in the catalytic dihydrogen generation process. Here we report the preparation and characterization of the pyridyl-phosphine mono-substituted complexes $(\mu\text{-pdt})[\text{Fe}_2(\text{CO})_5\text{L}]$ ($\text{L} = \text{Ph}_2\text{PCH}_2\text{Py}$, **3a**; Ph_2PPy , **3b**) and the disubstituted complexes $(\mu\text{-pdt})[\text{Fe}(\text{CO})_2(\text{PMe}_3)][\text{Fe}(\text{CO})_2\text{L}]$ ($\text{L} = \text{Ph}_2\text{PCH}_2\text{Py}$, **4a**; Ph_2PPy , **4b**, Chart 1), and the molecular structures of **3a**, **3b**, **4a**, **4b**, as well as the pyridyl-nitrogen protonated species $[\mathbf{3aH}_N][\text{OTf}]$ and $[\mathbf{3bH}_N][\text{OTf}]$. The doubly protonated species $[\mathbf{4bH}_\mu\text{H}_N]^{2+}$ containing a μ -hydride on the iron atoms and a proton on the pyridyl-nitrogen atom were detected by *in situ* IR, ^1H and ^{31}P NMR spectroscopy at low temperature. The spectroscopic evidence shows that the protonation of the Fe–Fe bond in **4b** is preferred over the pyridyl-nitrogen atom in the presence of HOTf. In addition, the electrochemical properties of **3a**, **3b**, and **4a** for proton reduction in the presence of different acids are also reported in this paper.

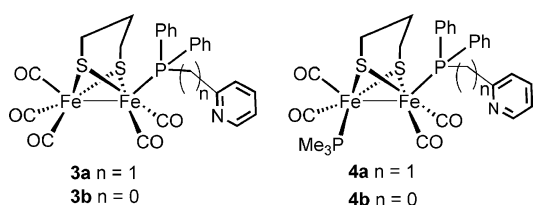


Chart 1

Table 1 IR data of the $\nu(\text{CO})$ bands for **3a**, $[\mathbf{3aH}_N][\text{OTf}]$, **3b**, $[\mathbf{3bH}_N][\text{OTf}]$, **4a**, and **4b**

Complex	$\nu(\text{CO})$ $\text{KBr}/\text{cm}^{-1}$	$\Delta\nu_{1\text{st}}(\text{CO})^a$ $\text{KBr}/\text{cm}^{-1}$
3a	2033(s), 1982(vs), 1956(vs), 1926(m)	
$[\mathbf{3aH}_N][\text{OTf}]$	2041(s), 1990(s), 1971(s), 1963(s), 1935(m)	8
3b	2039(vs), 2003(s), 1986(s), 1969(s), 1940(sh)	
$[\mathbf{3bH}_N][\text{OTf}]$	2049(vs), 1989(vs), 1972(sh), 1957(m), 1944(m)	10
4a	1976(s), 1945(s), 1907(s), 1884(m)	
4b	1982(s), 1947(vs), 1918(s), 1896(s)	

^a $\Delta\nu_{1\text{st}}(\text{CO}) = \nu_{1\text{st}}(\text{CO})_{\text{protonated}} - \nu_{1\text{st}}(\text{CO})_{\text{non-protonated}}$.

Results and discussion

Preparation and spectroscopic characterization of **3a**, **3b**, **4a**, **4b**, $[\mathbf{3aH}_N][\text{OTf}]$, and $[\mathbf{3bH}_N][\text{OTf}]$

Diiron dithiolate complexes **3a**, **3b**, **4a**, and **4b** containing pyridyl-phosphine ligands were prepared by CO displacement of $(\mu\text{-pdt})[\text{Fe}_2(\text{CO})_6]$ (**1**) and $(\mu\text{-pdt})[\text{Fe}_2(\text{CO})_5(\text{PMe}_3)]$ (**2**), respectively, in the presence of CO-removing reagent $\text{Me}_3\text{NO}\cdot 2\text{H}_2\text{O}$ in CH_3CN . Addition of 5 equiv. of HOTf to the Et_2O solution of **3a** and **3b** afforded pyridyl-nitrogen protonated species $[\mathbf{3aH}_N][\text{OTf}]$ and $[\mathbf{3bH}_N][\text{OTf}]$, respectively. All complexes were characterized by IR, MS, ^1H and ^{31}P NMR spectroscopy, and elemental analysis. The IR data of the $\nu(\text{CO})$ bands of **3a**, **3b**, **4a**, **4b**, $[\mathbf{3aH}_N][\text{OTf}]$, and $[\mathbf{3bH}_N][\text{OTf}]$ are summarized in Table 1. The frequencies of the first $\nu(\text{CO})$ bands of **3a** and **4a** are 6 cm^{-1} lower than their corresponding complexes **3b** and **4b**, implying a slightly stronger donating ability of $\text{Ph}_2\text{PCH}_2\text{Py}$ than Ph_2PPy . Protonation of **3a** and **3b** on the pyridyl-nitrogen atom causes a blue-shift of $8\text{--}10\text{ cm}^{-1}$ for the first $\nu(\text{CO})$ bands. The blue-shifts of the $\nu(\text{CO})$ bands for **3a** and **3b** are somewhat smaller than that ($15\text{--}20\text{ cm}^{-1}$) caused by protonation of the bridging nitrogen atom of analogous diiron complexes.^{3–5,9–12}

Protonation of **4b**

The red color of the CH_3CN solution of **4a** or **4b** quickly faded upon addition of HOTf at room temperature and all $\nu(\text{CO})$ bands disappeared in the IR spectrum, indicating the decomposition of the protonated diiron complexes. Due to the poor stability of the protonated species of **4a** and **4b** at room temperature, the protonation process of **4b** was studied by $^{31}\text{P}\{^1\text{H}\}$ and ^1H NMR spectroscopy in CD_2Cl_2 at $-55\text{ }^\circ\text{C}$.²⁵ Fig. 2 shows the variations of the ^{31}P (left) and ^1H (right) resonances in the selected regions with addition of 0–4 equiv. of HOTf to the solution of **4b**.

Complex **4b** displays two ^{31}P resonances at 64.2 ppm for Ph_2PPy and 26.2 ppm for PMe_3 (Fig. 2(a)). The relatively broad signal for PMe_3 at $-55\text{ }^\circ\text{C}$ indicates the slowdown of the rotation of the $\text{Fe}(\text{CO})_2(\text{PMe}_3)$ subunit. The similar case has been reported for $(\mu\text{-pdt})[\text{Fe}(\text{CO})_2(\text{PMe}_3)]_2$ by Darensbourg and coworkers.²⁶ When 1 equiv. of HOTf is added, a broad hydride signal at -14.5 ppm appears in the ^1H NMR spectrum (Fig. 2(b)), indicating the formation of the μ -hydride diiron complex $[\mathbf{4bH}_\mu]^+$.^{26–28} Concomitantly, two additional sharp signals at 62.8 ppm for Ph_2PPy and 21.3 ppm for PMe_3 appear in the $^{31}\text{P}\{^1\text{H}\}$ NMR spectrum (Fig. 2(b)). The protonation of the Fe–Fe bond results in high-field shifts of 4.9 and 1.4 ppm

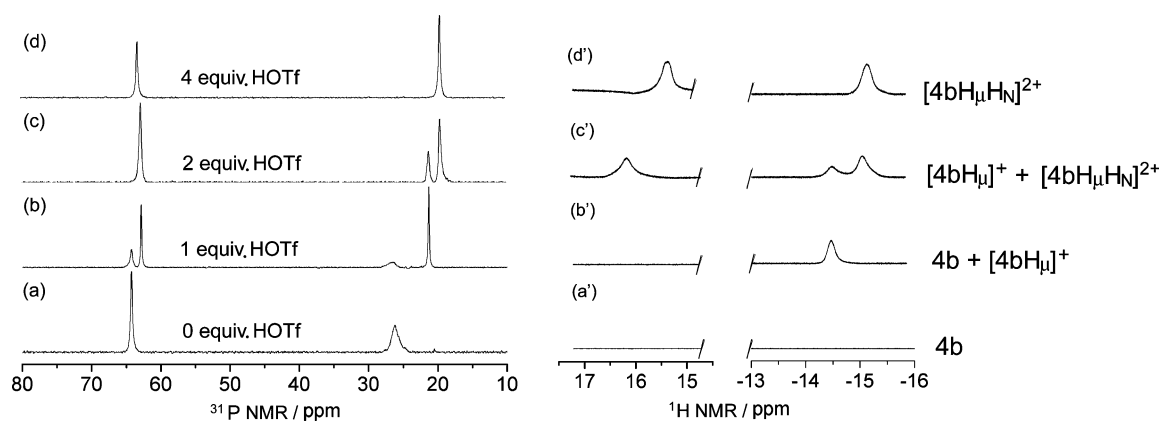


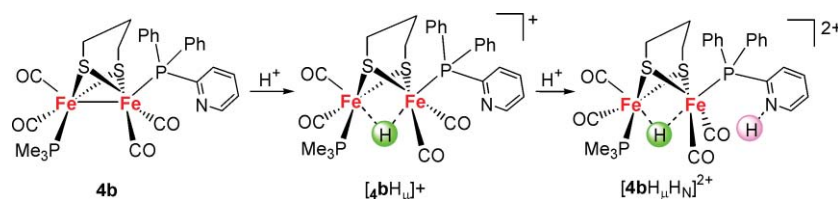
Fig. 2 Selected regions of $^{31}\text{P}\{^1\text{H}\}$ (left) and ^1H NMR (right) spectra for protonation of **4b** in CD_2Cl_2 at -55°C .

for the ^{31}P signals of PMe_3 and Ph_2PPy , respectively. Upon addition of 2 equiv. of HOTf, the appearance of two hydride signals at -14.5 and -15.2 ppm (Fig. 2(c')) gives unambiguous evidence for the existence of two types of μ -hydride species, that is, the μ -hydride complex $[\mathbf{4bH}_\mu]^+$ and the doubly protonated species $[\mathbf{4bH}_\mu\text{H}_\text{N}]^{2+}$ (see Scheme 1). An additional proton signal at 16.1 ppm is observed, which is ascribed to the proton on the pyridyl-nitrogen atom of $[\mathbf{4bH}_\mu\text{H}_\text{N}]^{2+}$. Simultaneously, the ^{31}P signals of **4b** completely disappears, accompanied with appearance of a new ^{31}P signal at 19.6 ppm in addition to the signal at 21.3 ppm for the PMe_3 ligand of $[\mathbf{4bH}_\mu]^+$ (Fig. 2(c)). The ^{31}P signal at 19.6 ppm is attributed to the PMe_3 ligand of $[\mathbf{4bH}_\mu\text{H}_\text{N}]^{2+}$. The ^{31}P signal at 62.8 ppm for Ph_2PPy in Fig. 2(c) does not show an observable shift, but the intensity of this signal relative to that of the ^{31}P NMR signal at 21.3 ppm in Fig. 2(c) apparently increases as compared to the intensity ratio of these two ^{31}P NMR signals in Fig. 2(b), suggesting an overlap of the ^{31}P NMR signals of the Ph_2PPy ligands in $[\mathbf{4bH}_\mu]^+$ and $[\mathbf{4bH}_\mu\text{H}_\text{N}]^{2+}$. When the accumulated quantity of HOTf is up to 4 equiv., the initial complex **4b** is quantitatively transformed to the doubly protonated species $[\mathbf{4bH}_\mu\text{H}_\text{N}]^{2+}$, suggested by the evidence that the signal at -14.5 ppm in Fig. 2(c') and the ^{31}P signal at 21.3 ppm in Fig. 2(c) completely disappears in Fig. 2(d') and (d). The broad signal for the proton on the pyridyl-nitrogen atom shifts from 16.1 to 15.4 ppm as the acidity of the solution is increased (Fig. 2(d')), and the ^{31}P signal for the Ph_2PPy ligand of $[\mathbf{4bH}_\mu\text{H}_\text{N}]^{2+}$ is slightly shifted to 63.1 ppm. The protonation of the pyridyl-nitrogen atom of $[\mathbf{4bH}_\mu]^+$ causes a high-field shift of the μ -hydride signal from -14.5 to -15.2 ppm. In contrast, the μ -hydride resonance in the doubly protonated species (μ -adtH)(μ -H)[$\text{Fe}(\text{CO})_2(\text{PMe}_3)_2$] (adt = *N*-benzyl-2-azapropane-1,3-dithiolato) is not affected by the protonation at the bridging nitrogen atom.^{3,4} The reason for the high-field shift of the μ -hydride resonance and for the relatively small shift of the ^{31}P signal of the

Ph_2PPy ligand upon protonation of the pyridyl-nitrogen atom of $[\mathbf{4bH}_\mu]^+$ are not clear up to now. The tentative explanation is that the protonation of the pyridyl-nitrogen atom results in a movement of the μ -hydride to the $\text{Fe}(\text{CO})_2(\text{PMe}_3)$ subunit with a strong donating ligand, which leads to the high-field shift of the μ -hydride resonance. Accordingly, the effect of the movement of μ -hydride to the $\text{Fe}(\text{CO})_2(\text{PMe}_3)$ subunit could partially offset the counter effect of the protonation at the pyridyl-nitrogen atom on the electron density of the $\text{Fe}(\text{CO})_2(\text{Ph}_2\text{PPy})$ subunit, resulting in a small shift of the ^{31}P signal for the Ph_2PPy ligand of $[\mathbf{4bH}_\mu\text{H}_\text{N}]^{2+}$ relative to the corresponding signal for $[\mathbf{4bH}_\mu]^+$.

The protonation process of **4b** in the presence of 0–4 equiv. of HOTf was also monitored by react-IR spectroscopy in CH_2Cl_2 at -55°C (Fig. S1 in ESI†). First, one equiv. of HOTf was added to the CH_2Cl_2 solution of **4b**, and when no change was observed from the IR spectra, one more equiv. of HOTf was immediately added. The selected IR spectra evincing the protonation process of **4b** are shown in Fig. 3.

Complex **4b** displays four $\nu(\text{CO})$ bands at 1985, 1951, 1916, and 1900 cm^{-1} (Fig. 3(a)). A large blue shift (*ca.* 77 wavenumbers) of the average value of the $\nu(\text{CO})$ bands is found upon addition of 1 equiv. of HOTf (Fig. 3(b)), which is indicative of the protonation of the Fe–Fe bond of **4b**.^{3,4,26–28} In contrast, the further addition of HOTf up to 4 equiv. results only in a slight blue shift (*ca.* 9 wavenumbers) of the $\nu(\text{CO})$ bands (Fig. 3(d)), suggesting that the singly protonated complex $[\mathbf{4bH}_\mu]^+$ is transformed to the doubly protonated species $[\mathbf{4bH}_\mu\text{H}_\text{N}]^{2+}$. The result from IR spectroscopic study further proves that in the presence of HOTf complex **4b** is protonated first at the Fe–Fe bond and then at the pyridyl-nitrogen atom in CH_2Cl_2 at low temperature. In contrast, protonation of **3a** and **3b** takes place at the pyridine-N atom and does not occur at the Fe–Fe bond. Compared with **3a** and **3b**, complex **4b** contains an additional good electron donating ligand PMe_3 , the electron



Scheme 1

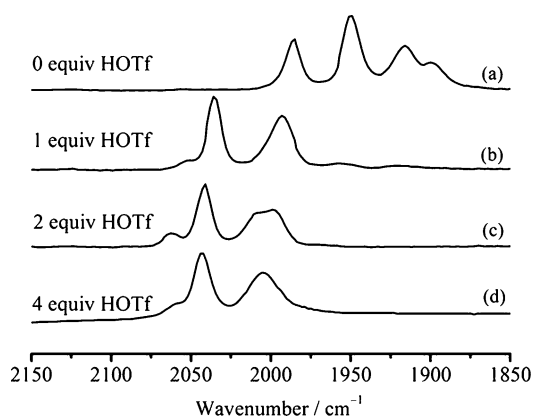


Fig. 3 Selected region of IR spectra of **4b** in the presence of 0–4 equiv. of HOTf in CH_2Cl_2 at -55°C .

density of the Fe–Fe bond in **4b** is much larger than that in **3a** and **3b**. This leads to the easy protonation of **4b** at the Fe–Fe bond in the presence of HOTf. The protonation order of **4b** is different from most of other reported analogous diiron complexes containing internal bases,^{3,5,28} in which protonation of the internal base is prior to the Fe–Fe bond. The only example which showed a similar protonation order as in our case was reported by Ott and co-workers for protonation of $(\mu\text{-adt})[\text{Fe}(\text{CO})_2(\text{PMe}_3)]_2$ (adt = N-benzyl-2-azapropane-1,3-dithiolato) in the presence of HCl.⁴ The proposed protonation process of **4b** is shown in Scheme 1.

Molecular structures of **3a**, **3b**, **4a**, **4b**, $[\mathbf{3aH}_N][\text{OTf}]$, and $[\mathbf{3bH}_N][\text{OTf}]$

The expected square-based-pyramidal coordination geometry is found for **3a**, **3b**, **4a**, **4b**, and the protonated species $[\mathbf{3aH}_N][\text{OTf}]$ and $[\mathbf{3bH}_N][\text{OTf}]$ according to the calculated structural factors (τ) for the iron atoms.²⁹ ORTEP diagrams for the crystal structures are shown in Fig. 4. Selected bond lengths, angles, and τ values are listed in Table 2. The X-ray analysis shows that the Ph_2PPy ligand in **3b** and $[\mathbf{3bH}_N][\text{OTf}]$ prefers an apical position to minimize the special crowd in the molecule, which is coincident with the reported structure for PPh_3 -monosubstituted complex $[(\mu\text{-pdt})\text{Fe}_2(\text{CO})_5(\text{PPh}_3)]$.¹⁹ In contrast, the $\text{Ph}_2\text{PCH}_2\text{Py}$ ligand in **3a** and $[\mathbf{3aH}_N][\text{OTf}]$ occupies a basal position with the CH_2Py group close to the apical CO ligand. The possible reason for the difference in the coordination position of the pyridyl-phosphine ligands,

$\text{Ph}_2\text{PCH}_2\text{Py}$ and Ph_2PPy , in **3a** and **3b** as well as in $[\mathbf{3aH}_N][\text{OTf}]$ and $[\mathbf{3bH}_N][\text{OTf}]$ is that the insertion of a CH_2 group to the bond between the phosphorus atom and the pyridyl ring decreases the steric interaction of the basal phosphine and the carbonyl ligands. Disubstituted complexes **4a** and **4b** both feature a basal/apical geometry with PMe_3 in a basal position and $\text{Ph}_2\text{PCH}_2\text{Py}$ or Ph_2PPy in an apical position.

Fig. 4(b and d) and the metric data for Fe \cdots N distances listed in Table 2 show that the orientation of the pyridyl-nitrogen atom in **3a** and **3b** is changed after protonation. The N–H \cdots O hydrogen bond among the pyridyl NH unit and the $[\text{HOTf}]^-$ anion accounts for the change of the pyridyl orientation. The Fe \cdots N distances in the solid state of **3a** and **3b** are 3.653(3) and 3.919(3) Å, respectively, while these distances are apparently enlarged by the rotation of the pyridyl group in the solid state of $[\mathbf{3aH}_N]^+$ and $[\mathbf{3bH}_N]^+$. Crystal packing diagrams and geometric data showing the hydrogen bonds in the crystalline state of $[\mathbf{3aH}_N][\text{OTf}]$ and $[\mathbf{3bH}_N][\text{OTf}]$ are given in Fig. S2 and S3 and Tables S1 and S2 in ESI.†

Electrochemical properties of **3a**, **3b**, and **4a**

The cyclic voltammograms (CVs) of **3a** and **3b** in the presence of different acids were measured to explore the role of the pyridyl-nitrogen atom in the electrocatalytic proton reduction process. The CVs of **3a** in the presence of HOAc and HOTf, and the plots of the current heights of electrocatalytic events vs. the concentration of acids in CH_3CN are given in Fig. 5 (For the CVs of **3b**, see Fig. S4 and S5). Complexes **3a** and **3b** display the first reductive events ($\text{Fe}^{\text{I}}\text{Fe}^{\text{I}}/\text{Fe}^{\text{I}}\text{Fe}^0$) at -1.86 and -1.83 V vs. Fc/Fc^+ , respectively, which are catalytically active for proton reduction in the presence of HOAc, while the electrocatalytic efficiencies of **3a** and **3b** are relatively low. The overpotentials for the electrocatalytic reduction of protons from HOAc are 400 mV for **3a** and 370 mV for **3b**.³⁰ Upon addition of 1 equiv. of HOTf, new reductive events are observed at -1.50 V for **3a** and -1.34 V for **3b** (Fig. S5 in ESI†). The positive shifts of 360–490 mV, resulting from the protonation of the pyridyl-nitrogen atoms of **3a** and **3b** in the presence of HOTf, are comparable to that (400–600 mV) caused by the protonation of the bridging nitrogen atom in the diiron 2-azapropane-1,3-dithiolate complexes.^{4,10,28} The current height of the new event at -1.50 V is enhanced in the same rate as that for the original event at -1.86 V with increase in the concentration of HOTf from 1 to 5 mM (Fig. 5(c)). The calculated value of ΔI_{av} is 16.3 μA per

Table 2 Selected bond lengths (Å) and angles ($^\circ$) for **3a**, $[\mathbf{3aH}_N][\text{OTf}]$, **3b**, $[\mathbf{3bH}_N][\text{OTf}]$, **4a**, and **4b**

Complex	3a	$[\mathbf{3aH}_N][\text{OTf}]$	3b	$[\mathbf{3bH}_N][\text{OTf}]$	4a	4b
Fe–Fe	2.5650(6)	2.5654(6)	2.5266(12)	2.5247(8)	2.5519(3)	2.5437(6)
Fe–P _{py}	2.2365(6)	2.2366(7)	2.2438(13)	2.2248(11)	2.2227(6)	2.2392(8)
Fe–P _{Me}	—	—	—	—	2.2342(7)	2.2385(9)
Fe \cdots N	3.919(3)	4.894(2)	3.653(3)	4.202(3)	4.060(2)	3.681(3)
P \cdots N	3.629(3)	3.548(2)	2.716(3)	2.809(3)	3.650(3)	2.692(3)
S \cdots S	3.038(1)	3.033(1)	3.048(2)	3.035(1)	3.028(1)	3.042(1)
S–Fe–S	84.78(3)	84.47(3)	84.67(4)	84.78(4)	84.41(2)	84.86(3)
	84.78(2)	85.20(3)	84.40(3)	84.18(4)	84.02(2)	83.64(2)
Fe–S–Fe	69.29(2)	69.50(3)	67.82(3)	67.84(4)	68.89(2)	68.40(2)
	69.49(2)	69.66(3)	67.72(3)	68.14(3)	68.78(2)	68.10(2)
S-2Fe–S	69.83(2)	69.56(3)	71.76(4)	71.65(4)	71.25(2)	71.75(3)
τ Fe(1)	0.005	0.080	0.342	0.296	0.089	0.058
τ Fe(2)	0.029	0.083	0.209	0.121	0.050	0.132

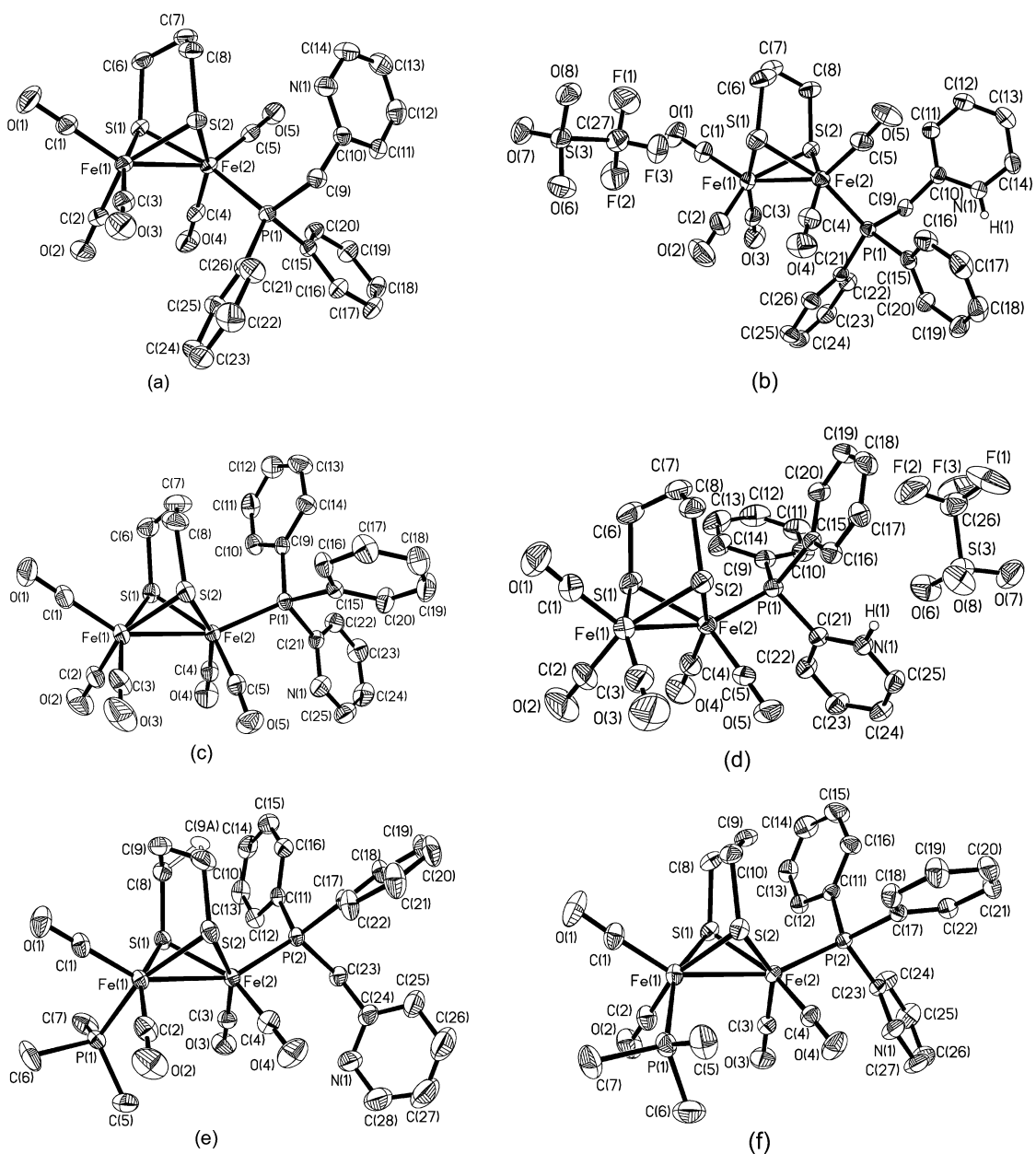


Fig. 4 ORTEP diagrams for **3a** (a), $[\mathbf{3aH}_N][\text{OTf}]$ (b), **3b** (c), $[\mathbf{3bH}_N][\text{OTf}]$ (d), **4a** (e), and **4b** (f). Hydrogen atoms are omitted for clarity except the proton on pyridyl-nitrogen atom in $[\mathbf{3aH}_N][\text{OTf}]$ and $[\mathbf{3bH}_N][\text{OTf}]$.

millimole of HOTf for both events, suggesting that the protonation of the internal base can effectively reduce the overpotential for proton reduction but not influence the electrocatalytic efficiency. The pyridyl-nitrogen atom in the phosphine ligand of **3a** and **3b** plays a role of the proton relay, similar to the function of the bridging nitrogen atom in the diiron azadithiolate complexes.^{4,10,28}

The effect of water on the electrocatalytic efficiency of **4a** was studied by the cyclic voltammetry in CH_3CN and in $\text{CH}_3\text{CN}-\text{H}_2\text{O}$ (50 : 1, v/v) mixed solution. Good CVs for **4a** and **4b** in the presence of HOTf are not obtained due to the poor stabilities of the doubly protonated species at room temperature. The electrochemical property of **4a** was studied in the presence of HOAc. Electrocatalytic proton reduction by **4a** occurs at -2.20 V in pure CH_3CN (Fig. 6(a)). Under this condition, the ΔI_{av} is

10.4 μA per millimole of HOAc according to slope 1 in Fig. 6(c). The second reductive event is tentatively ascribed to the reduction of an unknown product decomposed from the one-electron reduced species according to the previous report.³¹ The current height of the electrocatalytic event is considerably enhanced in $\text{CH}_3\text{CN}-\text{H}_2\text{O}$ (50 : 1, v/v, Fig. 6(b)). The electrocatalytic efficiency for proton reduction by **4a** in $\text{CH}_3\text{CN}-\text{H}_2\text{O}$ (50 : 1, v/v) increases *ca.* 5 times ($\Delta I_{av} = 51.6$ μA per millimole of HOAc, slope 2 in Fig. 6(c)) as compared to that in CH_3CN . This result is different from the previous report for the μ -hydride diphosphine-substituted diiron complex $[(\mu\text{-pdt})(\mu\text{-H})\{\text{Fe}(\text{CO})_2\text{PMe}_3\}_2][\text{BF}_4]$ and the PTA-substituted diiron complex $(\mu\text{-pdt})[\text{Fe}(\text{CO})_2(\text{PTA})]_2$ (PTA = 1,3,5-triaza-7-phosphaadamantane).³² The former displays no difference in the electrocatalytic efficiency for reduction of

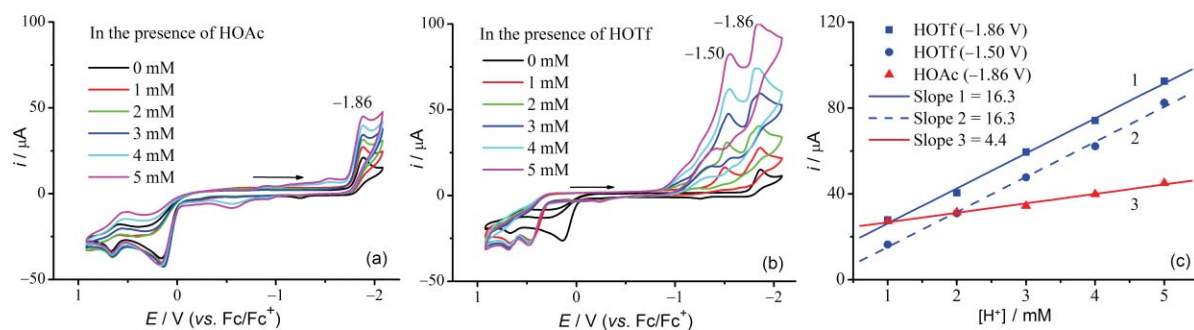


Fig. 5 Cyclic voltammograms of **3a** in the presence of (a) HOAc, (b) HOTf in CH_3CN , and (c) the plots of the current heights of electrocatalytic events vs. the concentration of acids.

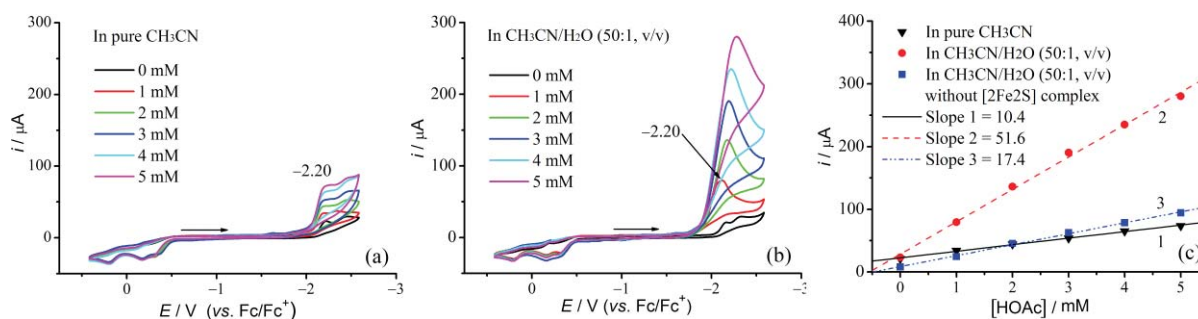


Fig. 6 Cyclic voltammograms of **4a** in the presence of HOAc, (a) in pure CH_3CN , (b) in $\text{CH}_3\text{CN}-\text{H}_2\text{O}$ (50:1, v/v), and (c) the plots of the current heights of electrocatalytic events vs. the concentration of acids.

protons from HOAc in pure CH_3CN or in $\text{CH}_3\text{CN}-\text{H}_2\text{O}$ mixture, and the electrocatalytic efficiency for the latter in $\text{CH}_3\text{CN}-\text{H}_2\text{O}$ (10:1 to 1:3, v/v) is enhanced less than twice as compared to that found in pure CH_3CN . To estimate the direct proton reduction of HOAc at the electrode, a control experiment was carried out in the absence of diiron complex, which shows that the ΔI_{av} is $17.4 \mu\text{A}$ in $\text{CH}_3\text{CN}-\text{H}_2\text{O}$ (50:1, v/v, slope 3 in Fig. 6(c)). It is not currently clear how a small amount of added water could apparently enhance the electrocatalytic efficiency of **4b** in the presence of HOAc.

Conclusions

In this work, a pyridyl group was introduced to the phosphine ligand of the diiron complex as a pendant basic site, which could approach to or stand apart from the μ -hydride of a protonated diiron complex by ligand and single bond rotation. Four diiron dithiolate complexes containing pyridyl-phosphine ligands and two corresponding protonated species were structurally characterized. The ^1H and ^{31}P NMR evidence at low temperature suggests that protonation of $(\mu\text{-pdt})[\text{Fe}(\text{CO})_2(\text{PMe}_3)][\text{Fe}(\text{CO})_2(\text{Ph}_2\text{PPy})]$ (**4b**) by HOTf occurs first at the Fe–Fe bond and then at the pyridyl-nitrogen atom. This result shows that the protonation process of diiron models can be readily alternated either by increasing the electron density of the iron centres,³³ or by adjusting the basicity of the internal base. Therefore, both the basicity and the relative position of the internal base to the hydride in a designed catalyst are important factors for hydrogen generation and uptake. The pyridyl group in the phosphine ligand of diiron complexes can act as a proton relay in the presence of strong acid just like the secondary amine in the diiron azadithiolate complexes does,

leading to the decrease of the overpotential for electrocatalytic proton reduction by 360–490 mV, and the hydrophilicity of the pyridyl group in the diiron complex renders the electrocatalytic efficiency more susceptible to water.

Experimental

Reagents and instruments

All manipulations related to pyridyl-phosphine ligands and organometallic complexes were performed using standard Schlenk technique under N_2 . Commercially available chemicals, 1,3-propanedithiol, $\text{Fe}(\text{CO})_5$, $\text{Me}_3\text{NO}\cdot 2\text{H}_2\text{O}$, picoline, 2-bromopyridine, and Ph_2PCL were reagent grade and used as received. The pyridyl-phosphine ligands, $\text{Ph}_2\text{PCH}_2\text{Py}$ ³⁴ and Ph_2PPy ,³⁵ diiron dithiolate complexes $[(\mu\text{-pdt})\{\text{Fe}(\text{CO})_3\}_2]$ (**1**)³⁶ and $[(\mu\text{-pdt})\{\text{Fe}_2(\text{CO})_5(\text{PMe}_3)\}]$ (**2**)¹⁹ were prepared according to literature methods. All organic solvents were distilled by standard methods and degassed prior to use. The ^1H and $^{31}\text{P}\{\text{H}\}$ NMR spectra were collected with a Bruker AVANCE II/400 spectrometer. Infrared spectra were recorded with a JASCO FT/IR 430 spectrophotometer. Elemental analyses were performed with an Elementar Vario EL III elemental analyzer. Mass spectra of iron complexes were recorded on an HP1100 MSD instrument.

Preparation of **3a**, **[3aH][OTf]**, **3b**, **[3b][OTf]**, **4a**, and **4b**

($\mu\text{-pdt})[\text{Fe}_2(\text{CO})_5(\text{Ph}_2\text{PCH}_2\text{Py})]$ (3a**).** One portion of $\text{Me}_3\text{NO}\cdot 2\text{H}_2\text{O}$ (0.11 g, 1 mmol) was added to a solution of $(\mu\text{-pdt})[\text{Fe}(\text{CO})_3]_2$ (**1**) (0.39 g, 1 mmol) in acetonitrile (30 mL) under N_2 . The mixture was stirred for 10 min, followed by the addition of the pyridyl-phosphine ligand $\text{Ph}_2\text{PCH}_2\text{Py}$ (0.28 g, 1 mmol) to

the solution. After 20 min, the volatiles were removed *in vacuo*. The resulting solid was purified by column chromatography on neutral alumina with hexane and CH_2Cl_2 as gradient eluents. The analytically pure solid of **3a** (0.44 g, 69%) was obtained as dark red powder. Crystals suitable for X-ray analysis were grown from a mixed solution of **3a** in hexane and CH_2Cl_2 at room temperature. Found: C, 48.93; H, 3.63; N, 2.17. $\text{C}_{26}\text{H}_{22}\text{Fe}_2\text{NO}_5\text{PS}_2$ requires C, 49.16; H, 3.49; N, 2.20%; $\nu_{\text{max}}(\text{KBr})/\text{cm}^{-1}$ 2033, 1982, 1956 and 1926 (CO); δ_{H} (400 MHz; CDCl_3) 8.43 (1 H, s, Py), 7.72–7.43 (10 H, 2 s, Ph), 7.33–6.42 (3 H, 3 s, Py), 4.10 (2 H, d, PCH_2), 1.85–1.50 (6 H, br m, $\text{SCH}_2\text{CH}_2\text{CH}_2\text{S}$); δ_{F} (400 MHz; CDCl_3) 64.24 (s, $\text{Ph}_2\text{PCH}_2\text{Py}$); $m/z(\text{APCI}^+)$ 636.0 (M + H^+).

$(\mu\text{-pdt})\text{Fe}_2(\text{CO})_5(\text{Ph}_2\text{PCH}_2\text{PyH})(\text{OTf})$ (3aH_N**||OTf)**. Anhydrous HOTf (12 μL , 0.13 mmol) was added to a stirring solution of **3a** (0.06 g, 0.1 mmol) in Et_2O (20 mL). The red precipitate immediately appeared. The mixture was stirred for 3 min, and then stood for 10 min. The upper layer of solvent was decanted. The deep red powder was collected and washed with Et_2O (5 \times 5 mL). The solid was dried *in vacuo* to give the protonated product **[3aH_N][OTf]** (0.04 g, 50%). Crystals suitable for X-ray diffraction were obtained by the direct diffusion of hexane to the concentrated CH_2Cl_2 solution of **[3aH_N][OTf]** over night at room temperature. Found: C, 41.55; H, 3.01; N, 2.03. $\text{C}_{27}\text{H}_{23}\text{F}_3\text{Fe}_2\text{NO}_8\text{PS}_3$ requires C, 41.29; H, 2.95; N, 1.78%; $\nu_{\text{max}}(\text{KBr})/\text{cm}^{-1}$ 2041, 1990, 1971, 1963 and 1935 (CO); δ_{H} (400 MHz; CDCl_3) 14.88 (1 H, s, NH), 8.54–7.76 (3 H, 3 s, Py), 7.70 (4 H, t, Ph), 7.55 (6 H, m, Ph), 7.33 (1 H, d, Py), 4.44 (2 H, d, PCH_2), 1.99–1.45 (6 H, m, $\text{SCH}_2\text{CH}_2\text{CH}_2\text{S}$); δ_{F} (400 MHz; CDCl_3) 64.31 (s, $\text{Ph}_2\text{PCH}_2\text{Py}$).

$(\mu\text{-pdt})[\text{Fe}_2(\text{CO})_5(\text{Ph}_2\text{PPy})]$ (3b**)**. Complex **3b** was prepared by using Ph_2PPy ligand with a similar procedure as that used for **3a**. The yield of **3b** is 77% (0.48 g). Found: C, 48.21; H, 3.33; N, 2.22. $\text{C}_{25}\text{H}_{20}\text{Fe}_2\text{NO}_5\text{PS}_2$ requires C, 48.33; H, 3.25; N, 2.25%;

$\nu_{\text{max}}(\text{KBr})/\text{cm}^{-1}$ 2039, 2003, 1986, 1969, 1940 and 1923 (CO); δ_{H} (400 MHz; CDCl_3) 8.79 (1 H, s, Py), 7.77 (5 H, d, Ph and Py), 7.52 (7 H, d, Ph and Py), 7.41 (1 H, s, Py), 1.77–1.55 (6 H, br m, $\text{SCH}_2\text{CH}_2\text{CH}_2\text{S}$); δ_{F} (400 MHz; CDCl_3) 66.70 (s, Ph_2PPy); $m/z(\text{APCI}^+)$ 621.8 (M + H^+).

$(\mu\text{-pdt})\text{Fe}_2(\text{CO})_5(\text{Ph}_2\text{PPyH})(\text{OTf})$ (3bH_N**||OTf)**. Protonated complex **[3bH_N][OTf]** (0.05 g, 62%) was obtained by the same procedure as for **[3aH_N][OTf]** but with **3b** as starting complex. Found: C, 40.27; H, 2.82; N, 1.88. $\text{C}_{26}\text{H}_{21}\text{F}_3\text{Fe}_2\text{NO}_8\text{PS}_3$ requires C, 40.49; H, 2.74; N, 1.82%; $\nu_{\text{max}}(\text{KBr})/\text{cm}^{-1}$ 2049, 1989, 1972, 1957 and 1944 (CO); δ_{H} (400 MHz; CD_2Cl_2) 14.68 (1 H, s, NH), 9.30–8.04 (4 H, 4 s, Py), 7.81–7.64 (10 H, 2 s, Ph), 1.94–1.37 (6 H, 3 s, $\text{SCH}_2\text{CH}_2\text{CH}_2\text{S}$); δ_{F} (400 MHz; CD_2Cl_2) 74.15 (s, Ph_2PPy).

$(\mu\text{-pdt})[\text{Fe}(\text{CO})_2(\text{PMe}_3)][\text{Fe}(\text{CO})_2(\text{Ph}_2\text{PCH}_2\text{Py})]$ (4a**)**. One portion of $\text{Me}_3\text{NO}\cdot 2\text{H}_2\text{O}$ (0.11 g, 1 mmol) was added to a solution of $(\mu\text{-pdt})[\text{Fe}_2(\text{CO})_5(\text{PMe}_3)]$ (**2**) (0.43 g, 1 mmol) in acetonitrile (30 mL) under N_2 at 35 °C. The mixture was stirred for 10 min, followed by addition of $\text{Ph}_2\text{PCH}_2\text{Py}$ (0.28 g, 1 mmol) to the solution. After 40 min, the volatiles were removed *in vacuo*. The resulting solid was purified by column chromatography on neutral alumina with hexane and CH_2Cl_2 as gradient eluents. The analytically pure solid of **4a** was collected as dark red powder (0.29 g, 43%). Crystals suitable for X-ray analysis were obtained by cooling the solution of **4a** in hexane and CH_2Cl_2 to –20 °C. Found: C, 49.31; H, 4.63; N, 2.03. $\text{C}_{28}\text{H}_{31}\text{Fe}_2\text{NO}_4\text{P}_2\text{S}_2$ requires C, 49.22; H, 4.57; N, 2.05%; $\nu_{\text{max}}(\text{KBr})/\text{cm}^{-1}$ 1976, 1945, 1907 and 1884 (CO). δ_{H} (400 MHz; CDCl_3) 8.37 (1 H, s, Py), 7.81(4 H, s, Ph), 7.42 (6 H, s, Ph), 7.34–6.65 (3 H, 3 s, Py), 4.18 (2 H, s, PCH_2), 1.74–1.54 (6 H, br m, $\text{SCH}_2\text{CH}_2\text{CH}_2\text{S}$), 1.45 (9 H, s, PMe_3); δ_{F} (400 MHz; CDCl_3) 59.15 (s, $\text{Ph}_2\text{PCH}_2\text{Py}$), 24.78 (s, PMe_3); $m/z(\text{APCI}^+)$ 684.0 (M + H^+).

Table 3 Crystallographic data and processing parameters for **3a**, **[3aH_N][OTf]**, **3b**, **[3bH_N][OTf]**, **4a**, and **4b**

Complex	3a	[3aH_N][OTf]	3b	[3bH_N][OTf]	4a	4b-0.5(C₆H₁₄)
Formula	$\text{C}_{26}\text{H}_{22}\text{Fe}_2\text{NO}_5\text{PS}_2$	$\text{C}_{27}\text{H}_{23}\text{F}_3\text{Fe}_2\text{NO}_8\text{PS}_3$	$\text{C}_{25}\text{H}_{20}\text{Fe}_2\text{NO}_5\text{PS}_2$	$\text{C}_{26}\text{H}_{21}\text{F}_3\text{Fe}_2\text{NO}_8\text{PS}_3$	$\text{C}_{28}\text{H}_{31}\text{Fe}_2\text{NO}_4\text{P}_2\text{S}_2$	$\text{C}_{30}\text{H}_{36}\text{Fe}_2\text{NO}_4\text{P}_2\text{S}_2$
M_w	635.24	785.31	621.21	771.29	683.30	712.36
Crystal system	Triclinic	Triclinic	Monoclinic	Monoclinic	Monoclinic	Triclinic
Space group	$P\bar{1}$	$P\bar{1}$	$P2_1/c$	$P2_1/c$	$P2_1/c$	$P\bar{1}$
$a/\text{\AA}$	9.0353(13)	10.8040(6)	9.285(6)	19.1778(6)	9.6520(2)	9.165(2)
$b/\text{\AA}$	12.3801(18)	10.9749(8)	17.400(11)	8.7364(3)	14.0097(3)	12.253(2)
$c/\text{\AA}$	12.7353(19)	14.5372(9)	16.844(11)	18.9530(6)	11.7256(3)	15.845(3)
$\alpha/^\circ$	97.723(2)	97.749(4)	90.00	90.00	90.00	82.194(2)
$\beta/^\circ$	108.443(2)	109.389(3)	103.196(9)	93.071(2)	103.012(1)	77.273(2)
$\gamma/^\circ$	91.284(2)	94.117(4)	90.00	90.00	90.00	73.081(2)
$V/\text{\AA}^3$	1335.9(3)	1598.53(18)	2650(3)	3170.92(18)	1544.84(6)	1655.6(6)
Z	2	2	4	4	2	2
μ/mm^{-1}	1.340	1.219	1.349	1.228	1.211	1.133
Crystal size/mm	$0.02 \times 0.07 \times 0.52$	$0.20 \times 0.22 \times 0.30$	$0.13 \times 0.40 \times 0.50$	$0.12 \times 0.25 \times 0.48$	$0.30 \times 0.30 \times 0.40$	$0.04 \times 0.07 \times 0.30$
θ range/ $^\circ$	2.20–26.97	1.89–27.63	2.25–29.01	2.13–27.50	1.78–30.00	1.74–26.00
Reflns collected	7773	15173	16207	14629	18855	9005
Unique data/Params	5618/334	7369/410	6432/322	7058/401	7618/362	6349/370
R_{int}	0.0109	0.0239	0.0374	0.0363	0.0213	0.0166
GOF on F^2	1.026	1.027	1.018	1.024	1.031	1.045
R_1^a $I > 2\sigma(I)$, all data	0.0305, 0.0389	0.0403, 0.0656	0.0398, 0.0702	0.0502, 0.1008	0.0291, 0.0344	0.0342, 0.0460
wR_2^b $I > 2\sigma(I)$, all data	0.0750, 0.0804	0.0935, 0.1065	0.0812, 0.0930	0.1096, 0.1317	0.0691, 0.0717	0.0805, 0.0860
Residual electron density/ $e \text{\AA}^{-3}$	0.586/–0.248	0.474/–0.350	0.591/–0.417	0.613/–0.336	0.426/–0.236	0.292/–0.320

^a $R_1 = \sum \|F_o\| - \|F_c\| / \sum \|F_o\|$. ^b $wR_2 = [\sum (w(F_o^2 - F_c^2)^2) / \sum w(F_o^2)^2]^{1/2}$. ^c The Flack parameter for **4a** in $P2_1$ is 0.016(10).

(μ -pdt)[Fe(CO)₂(PMe₃)][Fe(CO)₂(Ph₂PPy)] (**4b**). Complex **4b** was prepared using Ph₂PPy ligand with a similar procedure as that used for **4a**. The yield of **4b** is 52% (0.35 g). Found: C, 49.28; H, 4.79; N, 1.88. C₂₇H₂₉Fe₂NO₄P₂S₂·0.25C₆H₁₄ requires C, 49.55; H, 4.74; N, 2.03%; ν (KBr)/cm⁻¹ 1982, 1947, 1918 and 1896 (CO). δ_{H} (400 MHz; CDCl₃) 8.74 (1 H, s, Py), 7.86(4 H, s, Ph), 7.62 (2 H, s, Py), 7.41 (6 H, s, Ph), 7.24 (1 H, s, Py), 1.65–1.53 (6 H, br m, SCH₂CH₂CH₂S), 1.45 (9 H, s, PMe₃); δ_{F} (400 MHz; CDCl₃) 63.13 (s, Ph₂PPy), 24.84 (s, PMe₃); m/z (APCI+) 669.9 (M + H⁺).

Crystal structure determination of **3a**, [3aH_N][OTf], **3b**, [3bH_N][OTf], **4a**, and **4b**

The X-ray diffraction data were collected on a Bruker SMART Apex II CCD diffractometer at room temperature. Structures were solved by direct methods using SHELXTL-97 software package.³⁷ All non-hydrogen atoms were refined anisotropically. The hydrogen atoms on pyridyl-N in [3aH_N][OTf] and [3bH_N][OTf] were located by difference Fourier maps while other H atoms were placed at calculated positions and refined with fixed isotropic displacement parameters. Crystallographic data and processing parameters are summarized in Table 3.

Electrochemistry

Cyclic voltammograms were recorded on a BAS-100B electrochemical potentiostat using a three electrode cell at a scan rate of 100 mV s⁻¹ under argon atmosphere. The working electrode was a glass carbon disk (0.071 cm²) polished with 3 and 1 μm diamond pastes and sonicated in ion-free water for 10 min prior to use. The reference electrode was a non-aqueous Ag/Ag⁺ (0.01 M AgNO₃) in CH₃CN and the auxiliary electrode was a platinum wire. The acetonitrile (Aldrich, spectroscopy grade) used for electrochemical measurements was freshly distilled from CaH₂ under nitrogen. A solution of 0.05 M *n*Bu₄NPF₆ (Fluka, electrochemical grade) in CH₃CN was used as electrolyte. All potentials reported are *versus* Fc/Fc⁺ in CH₃CN.

Acknowledgements

We are grateful to the Chinese National Natural Science Foundation (Grant no. 20633020), the National Basic Research Program of China (Grant No. 2009CB220009), the Program for Changjiang Scholars and Innovative Research Team in University (IRT0711), the Swedish Energy Agency, the Swedish Research Council, and K and A Wallenberg Foundation for financial supports of this work.

References

- 1 J. W. Peters, W. N. Lanzilotta, B. J. Lemon and L. C. Seefeldt, *Science*, 1998, **282**, 1853–1858.
- 2 Y. Nicolet, C. Piras, P. Legrand, E. C. Hatchikian and J. C. Fontecilla-Camps, *Structure*, 1999, **7**, 13–23.
- 3 L. Schwartz, G. Eilers, L. Eriksson, A. Gogoll, R. Lomoth and S. Ott, *Chem. Commun.*, 2006, 520–522.

- 4 G. Eilers, L. Schwartz, M. Stein, G. Zampella, L. Gioia, S. Ott and R. Lomoth, *Chem.–Eur. J.*, 2007, **13**, 7075–7084.
- 5 B. E. Barton and T. B. Rauchfuss, *Inorg. Chem.*, 2008, **47**, 2261–2263.
- 6 W. Dong, M. Wang, X. Liu, K. Jin, G. Li, F. Wang and L. Sun, *Chem. Commun.*, 2006, 305–307.
- 7 H.-J. Fan and M. B. Hall, *J. Am. Chem. Soc.*, 2001, **123**, 3828–3829.
- 8 Z. Cao and M. B. Hall, *J. Am. Chem. Soc.*, 2001, **123**, 3734–3742.
- 9 J. D. Lawrence, H. Li, T. B. Rauchfuss, M. Bénard and M.-M. Rohmer, *Angew. Chem., Int. Ed.*, 2001, **40**, 1768–1771.
- 10 S. Ott, M. Kritikos, B. Åkermark, L. Sun and R. Lomoth, *Angew. Chem., Int. Ed.*, 2004, **43**, 1006–1009.
- 11 P. Das, J.-F. Capon, F. Gloaguen, F. Y. Pétillon, P. Schollhammer and J. Talarmin, *Inorg. Chem.*, 2004, **43**, 8203–8205.
- 12 F. Wang, M. Wang, X. Liu, K. Jin, W. Dong, G. Li, B. Åkermark and L. Sun, *Chem. Commun.*, 2005, 3221–3223.
- 13 E. J. Lyon, I. P. Georgakaki, J. H. Reibenspies and M. Y. Darensbourg, *Angew. Chem., Int. Ed.*, 1999, **38**, 3178–3180.
- 14 A. L. Cloirec, S. P. Best, S. Borg, S. C. Davies, D. J. Evans, D. L. Hughes and C. J. Pickett, *Chem. Commun.*, 1999, 2285–2286.
- 15 M. Schmidt, S. M. Contakes and T. B. Rauchfuss, *J. Am. Chem. Soc.*, 1999, **121**, 9736–9737.
- 16 J. D. Lawrence, T. B. Rauchfuss and S. R. Wilson, *Inorg. Chem.*, 2002, **41**, 6193–6195.
- 17 J. L. Nehring and D. M. Heinekey, *Inorg. Chem.*, 2003, **42**, 4288–4292.
- 18 J.-F. Capon, S. E. Hassnaoui, F. Gloaguen, P. Schollhammer and J. Talarmin, *Organometallics*, 2005, **24**, 2020–2022.
- 19 P. Li, M. Wang, C. He, G. Li, X. Liu, C. Chen, B. Åkermark and L. Sun, *Eur. J. Inorg. Chem.*, 2005, 2506–2513.
- 20 L. Schwartz, J. Ekström, R. Lomoth and S. Ott, *Chem. Commun.*, 2006, 4206–4208.
- 21 L. Duan, M. Wang, P. Li, Y. Na, N. Wang and L. Sun, *Dalton Trans.*, 2007, 1277–1283.
- 22 P.-Y. Orain, J.-F. Capon, N. Kervarec, F. Gloaguen, F. Pétillon, R. Pichon, P. Schollhammer and J. Talarmin, *Dalton Trans.*, 2007, 3754–3756.
- 23 L.-C. Song, M.-Y. Tang, S.-Z. Mei, J.-H. Huang and Q.-M. Hu, *Organometallics*, 2007, **26**, 1575–1577.
- 24 F. Xu, C. Tard, X. Wang, S. K. Ibrahim, D. L. Hughes, W. Zhong, X. Zeng, Q. Luo, X. Liu and C. J. Pickett, *Chem. Commun.*, 2008, 606–608.
- 25 Upon addition of HOTf to the CD₂Cl₂ solution of **4a** at –55 °C, precipitates appeared and the red color of the solution faded. The *in situ* IR and NMR measurements did not give any useful information for the protonation process of **4a**.
- 26 X. Zhao, I. P. Georgakaki, M. L. Miller, R. Mejia-Rodriguez, C.-Y. Chiang and M. Y. Darensbourg, *Inorg. Chem.*, 2002, **41**, 3917–3928.
- 27 X. Zhao, I. P. Georgakaki, M. L. Miller, J. C. Yarbrough and M. Y. Darensbourg, *J. Am. Chem. Soc.*, 2001, **123**, 9710–9711.
- 28 F. Wang, M. Wang, X. Liu, K. Jin, W. Dong and L. Sun, *Dalton Trans.*, 2007, 3812–3819.
- 29 F. I. Adam, G. Hogarth, I. Richards and B. E. Sanchez, *Dalton Trans.*, 2007, 2495–2498.
- 30 G. A. N. Felton, R. S. Glass, D. L. Lichtenberger and D. H. Evans, *Inorg. Chem.*, 2006, **45**, 9181–9184.
- 31 P. Li, M. Wang, C. He, G. Li, X. Liu, K. Jin and L. Sun, *Eur. J. Inorg. Chem.*, 2007, 3718–3727.
- 32 R. Mejia-Rodriguez, D. Chong, J. H. Reibenspies, M. P. Soriaga and M. Y. Darensbourg, *J. Am. Chem. Soc.*, 2004, **126**, 12004–12014.
- 33 F. Gloaguen, J. D. Lawrence, T. B. Rauchfuss, M. Bénard and M.-M. Rohmer, *Inorg. Chem.*, 2002, **41**, 6573–6582.
- 34 B. Åkermark, B. Krakenberger, S. Hansson and A. Vitagliano, *Organometallics*, 1987, **6**, 620–628.
- 35 T. J. Barder, F. A. Cotton, G. L. Powell, S. M. Tetrick and R. A. Walton, *J. Am. Chem. Soc.*, 1984, **106**, 1323–1332.
- 36 L. E. Bogan, D. A. Lesch and T. B. Rauchfuss, *J. Organomet. Chem.*, 1983, **250**, 429–438.
- 37 G. M. Sheldrick, *SHELX97*, University of Göttingen, Germany, 1998.